FINAL REPORT

Two-photon Absorption in Quantum Dots, quantum Dashes and Related Materials
PI: RAVINDER JAIN

DOE Grant: 2R368 – DE-FG02-02ER46015
Award Period: 9/1/02 – 8/31/09

Topic 1: Maximization of nonlinear fluorescence from ultrasmall (≤ 2 nm) semiconductor quantum dots to be used for deep tissue imaging (Key Participants: Li Wang, J.Y. Chen, D. Ancukiewicz, R.K. Jain)

Background and Need

Multiphoton absorption, particularly two-photon absorption (TPA), followed by fluorescence, has been identified as a useful technique for deep tissue imaging [1-3] for the study of several biological and biomedical processes, such as optical biopsy of *in vivo* human skin [2], angiography [4], embryonic development in hamsters [5], intravital measurement of gene expression in mice tumors [6], and intravital studies of mouse and rat brains [7, 8] and kidneys [9]. The advantages of two-photon absorption-induced fluorescence (TPAF) imaging stem not only from the larger depths of penetration [10, 11] that are obtainable at the longer wavelengths inevitably used for excitation, but also from the ease of filtering the near-IR TPAF excitation from the visible or near-UV fluorescence emission, and the higher spatial resolutions inherent in multiphoton microscopy [12].

For tissue specimens in which the use of labeling is necessary, the use of semiconductor quantum dots (SQDs) as biological labels [13, 14] – in comparison with fluorescent dyes [15] – is particularly desirable because of (i) their photochemical stability [16], (ii) their ability to be tuned over broad wavelength ranges [17], and (iii) their amenability to bio-conjugation [18-22]. Several researchers [4, 23, 24] have also demonstrated that SQDs exhibit very large TPA coefficients, particularly in comparison to those of dyes used for TPAF-based imaging. In most previous studies using SQDs for TPAF imaging of biological tissues [4, 25], relatively large SQDs (diameter $d \geq 5$ nm) have been used because their TPA coefficients are much larger those of smaller SQDs of the same material composition [24]. In particular, Larson et al [4] have demonstrated that the two-photon "action cross-sections" (product of the TPA cross section and the fluorescence quantum efficiencies) of CdSe/ZnS SQDs are over 3 orders of magnitude higher than those of conventional dye-based fluorescent probes (such as fluorescein isothiocyanate (FITC)-dextran), with measured values as high as 47,000 Goeppert -Mayer (GM) units. These authors also demonstrated visualization of capillaries hundreds of micrometers deep through the skin of living mice with such SQD-based TPAF probes.

In addition, even though most of the studies of bio-imaging based on quantum dot labels have used relatively large SQDs ($d \geq 5$ nm) [4, 14, 25-31], there are numerous biological imaging studies in which the use of much smaller SQDs is critical. These include deep-tissue wavelength-multiplexed multicolor imaging [28, 31] in which smaller SQDs of the same material lead to fluorescence at shorter wavelengths ("bluer") and

applications involving intra-nuclear studies of cells [26, 27, 29, 30] *in which much smaller SQDs are critical for effective penetration of the sub-10 nm nuclear pores [30].*

Experimental Setup and Related Details

A mode-locked Ti-sapphire laser of 200 fs pulsewidth and 76 MHz repetition rate was used as the excitation source to characterize the TPAF signals. As shown in Fig. 1, a concave mirror of 10 cm focal length was used to focus the 2 mm diameter laser beam to a spot size of 80 μm into a colloidal USQD suspension ("sample") placed in a cuvette of 2 mm pathlength.

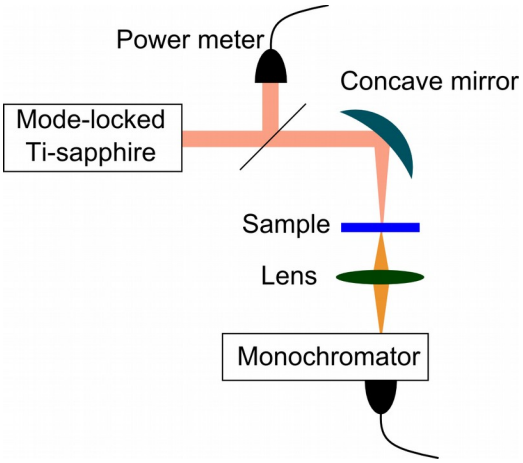

Fig. 1. Experimental setup used to characterize TPAF signals from CdSe/ZnS USQDs.

Standard lock-in detection techniques were used to measure the TPAF signals collected by a photomultiplier tube (PMT) at the exit port of a half-meter monochromator with a slit width of 2 mm, corresponding to a spectral resolution of ~ 3 nm. For this study, we used CdSe/ZnS (core/shell) USQDs of core diameter d ~ 2 nm in toluene, with a specified size variation of less than 5%; the total physical diameter of the USQDs is ~ 3.2 nm when ZnS shell are also taken into account [33].

Results and Discussion

In order to interpret the TPAF data (taken with the experimental setup of Fig. 1) accurately, it is important to characterize the USQD samples in terms of their "baseline" linear optical and physical properties. The single photon absorption spectrum of these USQDs is shown in Fig. 2(a), with a peak at ~ 460 nm and a full width at half maximum (FWHM) of ~ 40 nm. Also as seen in Fig. 2(a), the linear fluorescence spectrum exhibits a peak emission wavelength of ~ 496 nm and a FWHM of ~ 30 nm. This emission spectrum was obtained by using either a 325 nm He-Cd laser or the second harmonic generation of our mode-locked Ti-sapphire laser as the excitation source, and no significant difference was noted in the emission spectra for these two excitation sources. The peak locations of these spectra are consistent with those expected [33] from CdSe SQDs with a core diameter of 2 nm, and the FWHMs of these spectra confirm a size

variation of less than 5% and the absence of aggregation [34] in these USQD samples. It is useful to note that no significant changes in the spectra -- nor any other sign of aggregation -- was noted even after these USQD samples were stored in the lab at room temperature for over a month.

We also examined these USQD samples with a transmission electron microscope (TEM). A typical TEM image is shown in Fig. 2(b); in this image, the darker spots correspond to individual SQDs. Because of the lack of sufficient resolution and the low contrast in these TEM images (typical with CdSe/ZnS SQDs), it was difficult to accurately resolve the exact size of our SQDs. Nevertheless, it is easy to estimate an upper limit of about 4 nm for the "particles" (darker dots) seen more predominantly in the lower right quadrant of these TEM images, and to confirm the general lack of aggregation of these particles. Note that the "sub-nm" type of finer grain structure seen in this TEM image is an artifact of the imaging setup. The fact that the darker dots were not artifacts of our TEM imaging setup, and corresponded to the anticipated quantum dots was verified with an XRD analysis; the data from this analysis confirmed the existence of all the anticipated elemental compounds (Cd, Se, Zn, S).

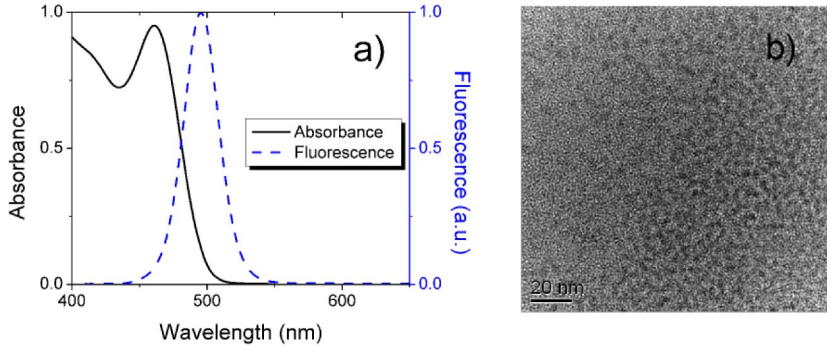

Fig. 2. (a) Linear absorption (peak at 460 nm and FWHM of 40 nm) and fluorescence (peak at ~ 496 nm and FWHM of 30 nm) spectra of 2 nm CdSe/ZnS USQDs. The absorbance corresponds to a 2 mm path length solution at a concentration of 1.4 mg/ml; (b) a typical TEM image of the CdSe/ZnS USQDs used in this study. The darker dots that are predominantly in the lower left hand area (below the NE to SW diagonal) are the CdSe SQDs, whereas the finer "sub-nm" type of graininess in the image is due to an artifact of the TEM imaging setup.

Note that the emission spectra from the ZnS shell (peak wavelength > 335 nm) and the capping layer are both located at wavelengths far from the emission spectra of the CdSe USQDs. Nevertheless, in order to confirm that the ZnS and capping layers provide negligible amounts of contribution to the CdSe USQD emission spectrum of Fig. 2(a), we studied the emission spectra from a range of CdSe/ZnS SQD samples containing dots of varying sizes, as shown in Fig. 3 below. Any emission from the ZnS shell and capping layers would show up as an extraneous "common" feature in each of these spectra; the

lack of any such common emission spectrum confirms the absence of any interfering emission from the ZnS shell and the capping layers in this spectral region.

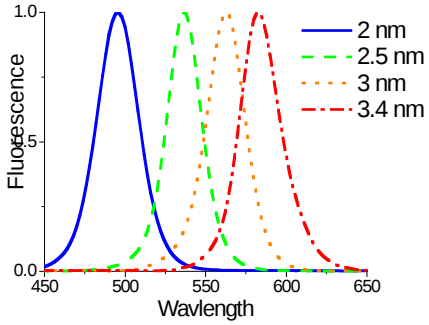

Fig. 3. Linear fluorescence from four different CdSe/ZnS SQD colloidal samples, corresponding to SQDs of distinct average sizes varying from 2 nm to 3.4 nm

We next used the experimental setup of Fig. 1 to measure TPAF spectra for several distinct excitation wavelengths in the 750 nm to 950 nm range while keeping the excitation intensity constant (~ 8 GW/cm^2). Six representative spectra in the 810 nm to 860 nm range are shown in Fig. 4. The spectral shapes and the peak wavelengths of the TPAF emission spectra were very similar to those observed with single photon excitation, and showed a negligible change (≤ 5%) as a function of the excitation wavelength.

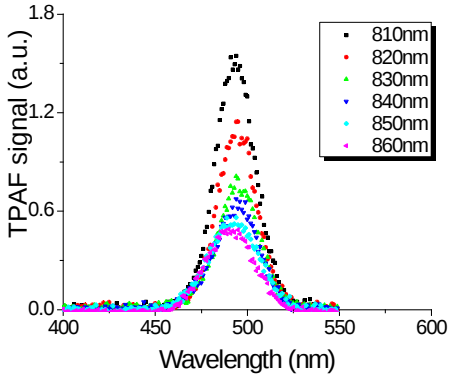

Fig. 4. TPAF spectra for several distinct excitation wavelengths in the 810 nm - 860 nm range, using a constant excitation intensity of 8 GW/cm^2. The vertical axis corresponds to the signals obtained with the lock-in amplifier when the PMT is located at the exit of the monochromator.

In order to verify that the observed fluorescence emission was caused by a two-photon absorption process, we measured the dependence of the fluorescence power on the excitation intensity (Fig. 5). This was done by removing the monochromator and measuring the power in the entire spectrum ("area under the curve") at the photomultiplier, while introducing a short-pass optical filter (Schott BG 39) to block any contributions to the PMT signal from any stray scattered light from the Ti-sapphire laser.

Log-log plots of the fluorescence power ("TPAF signal") as a function of the excitation intensity are shown in Fig. 5 for two representative wavelengths, 810 nm (dots) and 930 nm (triangles). The slopes of the fitting lines (dashed for 810 nm and solid for 930 nm) are 2.0 (+/-0.15) and 1.9 (+/-0.15), confirming that the measured fluorescence emission was caused by a TPA process.

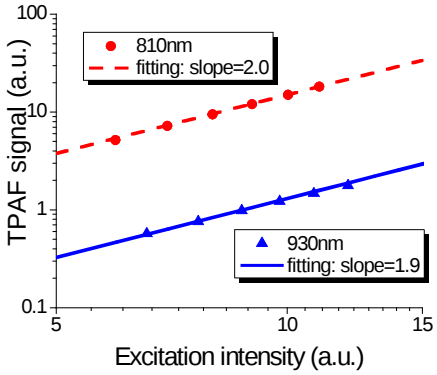

Fig. 5. Power in the TPA-induced fluorescence as a function of the excitation intensity for excitation at 810 nm and 930 nm respectively. The vertical axis corresponds to the lock-in amplifier signal when the entire fluorescence spectrum (no monochromator) is focused on the PMT, and a value of 12 on the horizontal axis corresponds to an intensity of ~ 8 GW/cm^2.

We next measured the "integrated" (over the entire emission spectrum) optical power in the TPAF emission as a function of the excitation wavelength while keeping the excitation intensity at each excitation wavelength constant (at 8 GW/cm^2). Fig. 6 shows the result of such measurements for two different SQD concentrations (1.4 mg/mL and 0.4 mg/mL of CdSe). These plots depict strong resonant enhancement in the TPAF signals at excitation wavelengths close to 780 nm; for the more concentrated sample, the TPAF signal at 780 nm is ~ 8 times that at 850 nm and ~ 68 times that at 900 nm. Note that when the experiment was

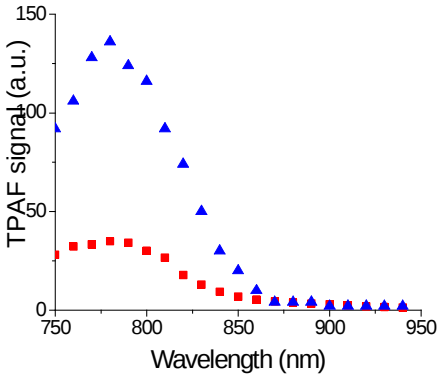

Fig. 6. The wavelength dependence of the TPA-induced fluorescence outputs for the 2 nm CdSe/ZnS USQDs at two different concentrations (1.4 mg/mL: blue triangles; 0.4 mg/mL: red squares).

repeated with just the solvent (without any SQDs therein), there was no measurable fluorescence, indicating that there was no "background" fluorescence attributable to the solvent, and the measured TPAF signals are entirely due to the USQDs themselves. Note also that although lower USQD concentrations may be preferred for some biological studies, the higher concentration (1.4 mg/ml) is within the range of concentrations that may be usable for several biological imaging experiments. Nevertheless, ***these experiments clearly illustrate that with these USQDs for TPAF-based deep-tissue imaging, the use of an excitation wavelength of 780 nm is optimal, with signal enhancements as much as 68 times over those obtained at an excitation wavelength of 900 nm.*** Note also that most tissue of interest is highly transparent at 780 nm, and that this wavelength is still conducive to high-resolution deep-tissue imaging.

It is interesting to note that the excitation wavelength at the TPAF peak is not exactly twice of the peak wavelength for linear absorption: the TPAF peak is observed to occur at about 780 nm, which is shorter than that expected based on the peak wavelength (~ 460 nm) of the linear absorption. Such a wavelength difference can be accounted for by considering the role of different transitions and selection rules associated with single photon absorption and TPA. It is well known that the selection rules are different for single photon absorption and TPA in semiconductor interband transitions [35]: single photon transitions satisfy $\Delta L = 0, \pm 2$ and $\Delta F = 0, \pm 1$ and two-photon transitions satisfy $\Delta L = \pm 1, \pm 3$ and $\Delta F = 0, \pm 1, \pm 2$ (where F is the total angular momentum). Although such selection rules are not strictly followed in USQDs because of band-mixing effects, the magnitude of the cross sections might still differ significantly, i.e., TPA transitions with $\Delta L = \pm 1, \pm 3$ and $\Delta F = 0, \pm 1, \pm 2$ have much larger cross sections than those with $\Delta L = 0, \pm 2$ and $\Delta F = 0, \pm 1$ [36].

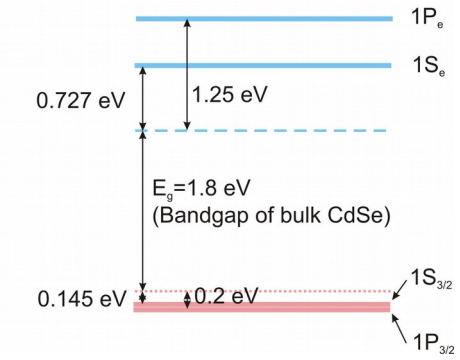

Fig. 7. Schematic of the electronic energy levels for CdSe/ZnS quantum dots of 2 nm diameter. (see ref [37] for details)

To identify the energy levels inside this particular USQD system (λ_{abs} = 460 nm), an 8-band Pidgeon & Brown model was employed to calculate the energy levels positions [37]. Fig. 7 schematically shows the lowest two levels in the conduction and valence

bands. The bandgap of bulk semiconductor CdSe is 1.8 eV, with the dashed blue and the dotted red lines indicating the bottom of the conduction band and the top of the valence band, respectively. The two hole energy levels closest to the band edge are $1S_{3/2}$ (0.145 eV below the band edge) and $1P_{3/2}$ (0.2 eV below the band edge), and the two electron energy levels closest to the band edge are $1S_e$ (0.727 eV above the band edge) and $1P_e$ (1.25 eV above the band edge), respectively. Thus the transition $1S_{3/2} \Rightarrow 1S_e$ gives the lowest single photon peak absorption energy (2.672 eV or 464 nm), which matches our experimental data (460 nm: peak absorption wavelength for single photon excitation) quite well, while the transition $1S_{3/2} \Rightarrow 1P_e$ corresponds to a TPA photon energy (3.195 eV or 776 nm for TPA) that also matches our experimental data (780 nm wavelength of the TPA peak) well.

One potential problem of using USQDs in biomedical imaging applications is that the emission spectrum may be too close to or may even overlap with that of autofluorescence in tissues. Fortunately, the TPAF signals from SQDs are much stronger than the TPA signals from autofluorescence in tissues. The TPA cross sections of SQDs can be as high as 47,000 GM units [4], and the TPA cross sections estimated for our USQDs are ~ 7,000 GM units based on an open aperture z-scan measurement, while the TPA cross sections for autofluorescence in tissues are only of the order of a few GM [38].

Summary of our Studies

We have proposed the use of USQDs for various deep-tissue biological imaging applications, notably wavelength-multiplexed multicolor imaging and intra-nuclear studies such as those involving cell apoptosis, and have studied the issue of maximizing TPAF signals from CdSe/ZnS USQDs to be used for this application. In particular, using 2 nm USQDs, we have shown that the TPAF signal at 780 nm is ~ 8 times that at 850 nm and 68 times that at 900 nm, two wavelengths that have been used in previous studies using CdSe/ZnS SQDs for deep-tissue imaging of biological studies via TPAF [4].

References

1. W. Denk, J. H. Strickler, and W. W. Webb, "Two-photon laser scanning fluorescence microscopy," Science **248**, 73-76 (1990).
2. B. R. Masters, P. T. C. So, and E. Gratton, "Optical biopsy of in vivo human skin: Multi-photon excitation microscopy," Lasers Med. Sci. **13**, 196-203 (1998).
3. R. M. Williams, W. R. Zipfel, and W. W. Webb, "Multiphoton microscopy in biological research," Curr. Opin. Chem. Biol. **5**, 603-608 (2001).
4. D. R. Larson, W. R. Zipfel, R. M. Williams, S. W. Clark, M. P. Bruchez, F. W. Wise, and W. W. Webb, "Water-soluble quantum dots for multiphoton fluorescence imaging in vivo," Science **300**, 1434-1436 (2003).
5. J. M. Squirrell, D. L. Wokosin, J. G. White, and B. D. Bavister, "Long-term two-photon fluorescence imaging of mammalian embryos without compromising viability," Nat. Biotechnol. **17**, 763-767 (1999).
6. E. B. Brown, R. B. Campbell, Y. Tsuzuki, L. Xu, P. Carmeliet, D. Fukumura, and R. K. Jain, "In vivo measurement of gene expression, angiogenesis and physiological function in tumors using multiphoton laser scanning microscopy," Nat. Med. **7**, 864-868 (2001).
7. K. Svoboda, W. Denk, D. Kleinfeld, and D. W. Tank, "In vivo dendritic calcium dynamics in neocortical pyramidal neurons," Nature **385**, 161-165 (1997).
8. B. E. Chen, B. Lendvai, E. A. Nimchinsky, B. Burbach, K. Fox, and K. Svoboda, "Imaging high-resolution structure of GFP-expressing neurons in neocortex in vivo," Learn. Memory **7**, 433-441 (2000).
9. K. W. Dunn, R. M. Sandoval, K. J. Kelly, P. C. Dagher, G. A. Tanner, S. J. Atkinson, R. L. Bacallao, and B. A. Molitoris, "Functional studies of the kidney of living animals using multicolor two-photon microscopy," Am. J. Physiol.: Cell Physiol. **283**, C905-916 (2002).
10. V. E. Centonze, and J. G. White, "Multiphoton excitation provides optical sections from deeper within scattering specimens than confocal imaging," Biophys. J. **75**, 2015-2024 (1998).
11. X. Deng, and M. Gu, "Penetration depth of single-, two-, and three-photon fluorescence microscopic imaging through human cortex structures: Monte Carlo simulation," Appl. Opt. **42**, 3321-3329 (2003).
12. L. Sacconi, R. P. O'Connor, A. Jasaitis, A. Masi, M. Buffelli, and F. S. Pavone, "In vivo multiphoton nanosurgery on cortical neurons," J. Biomed. Opt. **12**, 050502 (2007).
13. M. Bruchez, Jr., M. Moronne, P. Gin, S. Weiss, and A. P. Alivisatos, "Semiconductor nanocrystals as fluorescent biological labels," Science **281**, 2013-2016 (1998).
14. W. C. W. Chan, and S. Nie, "Quantum dot bioconjugates for ultrasensitive nonisotopic detection," Science **281**, 2016-2018 (1998).
15. M. J. O'Donovan, S. Ho, G. Sholomenko, and W. Yee, "Real-time imaging of neurons retrogradely and anterogradely labelled with calcium-sensitive dyes," J. Neurosci. Methods **46**, 91-106 (1993).

16. M. Danek, K. F. Jensen, C. B. Murray, and M. G. Bawendi, "Synthesis of luminescent thin-film CdSe/ZnSe quantum dot composites using CdSe quantum dots passivated with an overlayer of ZnSe," Chem. Mater. **8**, 173-180 (1996).
17. C. B. Murray, D. J. Norris, and M. G. Bawendi, "Synthesis and characterization of nearly monodisperse CdE (E = S, Se, Te) semiconductor nanocrystallites," J. Am. Chem. Soc. **115**, 8706-8715 (1993).
18. P. T. Tran, E. R. Goldman, G. P. Anderson, J. M. Mauro, and H. Matroussi, "Use of luminescent CdSe-ZnS nanocrystal bioconjugates in quantum dot-based nanosensors," (Wiley-VCH, Germany, 2002), pp. 427-432.
19. D. Gerion, F. Pinaud, S. C. Williams, W. J. Parak, D. Zanchet, S. Weiss, and A. P. Alivisatos, "Synthesis and properties of biocompatible water-soluble silica-coated CdSe/ZnS semiconductor quantum dots," J. Phys. Chem. B **105**, 8861-8871 (2001).
20. W. J. Parak, D. Gerion, D. Zanchet, A. S. Woerz, T. Pellegrino, C. Micheel, S. C. Williams, M. Seitz, R. E. Bruehl, Z. Bryant, C. Bustamante, C. R. Bertozzi, and A. P. Alivisatos, "Conjugation of DNA to silanized colloidal semiconductor nanocrystalline quantum dots," Chem. Mater. **14**, 2113-2119 (2002).
21. S. Wang, N. Mamedova, N. A. Kotov, W. Chen, and J. Studer, "Antigen/Antibody immunocomplex from CdTe nanoparticle bioconjugates," Nano Lett. **2**, 817-822 (2002).
22. W. Guo, J. J. Li, Y. A. Wang, and X. Peng, "Conjugation chemistry and bioapplications of semiconductor box nanocrystals prepared via dendrimer bridging," Chem. Mater. **15**, 3125-3133 (2003).
23. L. Wang, Z. Zhang, R. K. Jain, F. Vanholsbeeck, S. Murdoch, and J. Harvey, "Measurement of two-photon absorption coefficients in colloidal semiconductor quantum dots," in *Proceedings of IEEE Lasers and Electro-Optics Society Annual Meeting*, Vol. # 2, (Institute of Electrical and Electronics Engineers Inc., New York, NY, 2004), pp. 487-488.
24. S.-C. Pu, M.-J. Yang, C.-C. Hsu, C.-W. Lai, C.-C. Hsieh, S. H. Lin, Y.-M. Cheng, and P.-T. Chou, "The empirical correlation between size and two-photon absorption cross section of CdSe and CdTe quantum dots," Small **2**, 1308-1313 (2006).
25. M. J. Levene, D. A. Dombeck, K. A. Kasischke, R. P. Molloy, and W. W. Webb, "In vivo multiphoton microscopy of deep brain tissue," J. Neurophysiol. **91**, 1908-1912 (2004).
26. F. Chen, and D. Gerion, "Fluorescent CdSe/ZnS nanocrystal-peptide conjugates for long-term, nontoxic imaging and nuclear targeting in living cells," Nano Lett. **4**, 1827-1832 (2004).
27. J. G. D. Foley, and J. B. L. Bard, "Apoptosis in the cortex of the developing mouse kidney," J. Anat. **201**, 477-484 (2002).
28. W. Jiang, A. Singhal, J. Zheng, C. Wang, and W. C. W. Chan, "Optimizing the synthesis of red- to near-IR-emitting CdS-capped $CdTe_xSe_{1-x}$ alloyed quantum dots for biomedical imaging," Chem. Mater. **18**, 4845-4854 (2006).
29. I. Nabiev, S. Mitchell, A. Davies, Y. Williams, D. Kelleher, R. Moore, Y. K. Gun'ko, S. Byrne, Y. P. Rakovich, J. F. Donegan, A. Sukhanova, J. Conroy, D. Cottell, N. Gaponik, A. Rogach, and Y. Volkov, "Nonfunctionalized nanocrystals

can exploit a cell's active transport machinery delivering them to specific nuclear and cytoplasmic compartments," Nano Lett. **7**, 3452-3461 (2007).
30. Y. Xu, Q. Wang, P. He, Q. Dong, F. Liu, Y. Liu, L. Lin, H. Yan, and X. Zhao, "Cell nucleus penetration by quantum dots induced by nuclear staining organic fluorophore and UV-irradiation," Adv. Mater. **20**, 3468-3473 (2008).
31. K.-T. Yong, I. Roy, H. E. Pudavar, E. J. Bergey, K. M. Tramposch, M. T. Swihart, and P. N. Prasad, "Multiplex imaging of pancreatic cancer cells by using functionalized quantum rods," Adv. Mater. **20**, 1412-1417 (2008).
32. L. Wang, D. Ancukiewicz, J. Y. Chen, and R. K. Jain, "Surface-plasmon enhanced fluorescence in CdSe/ZnS semiconductor quantum dots," Paper # CTu07, presented at the Conference on Lasers and Electro-Optics Conference (CLEO/IQEC 2009), Baltimore, MD, 31 May, 2009
33. All the SQD samples described here were purchased from Evident Technologies; the "2 nm" USQD samples used in this study are their "Blue" product with a specified CdSe core diameter of 1.9 nm (+/- 5%) and a peak emission wavelength of 490 nm, consistent with our measurements reported here.
34. Z. Tang, N. A. Kotov, and M. Giersig, "Spontaneous organization of single CdTe nanoparticles into luminescent nanowires," Science **297**, 237-240 (2002).
35. K. I. Kang, B. P. McGinnis, Sandalphon, Y. Z. Hu, S. W. Koch, N. Peyghambarian, A. Mysyrowicz, L. C. Liu, and S. H. Risbud, "Confinement-induced valence-band mixing in CdS quantum dots observed by two-photon spectroscopy," Phys. Rev. B **45**, 3465-3468 (1992).
36. M. E. Schmidt, S. A. Blanton, M. A. Hines, and P. Guyot-Sionnest, "Size-dependent two-photon excitation spectroscopy of CdSe nanocrystals," Phys. Rev. B **53**, 12629-12632 (1996).
37. A. L. Efros, and M. Rosen, "Electronic structure of semiconductor nanocrystals," Annu. Rev. Mater. Sci. **30**, 475-521 (2000).
38. N. J. Durr, T. Larson, D. K. Smith, B. A. Korgel, K. Sokolov, and A. Ben-Yakar, "Two-photon luminescence imaging of cancer cells using molecularly targeted gold nanorods," Nano Lett. **7**, 941-945 (2007).
39. B. I. Tarnowski, F. G. Spinale, and J. H. Nicholson, "DAPI as a useful stain for nuclear quantitation," Biotech. Histochem. **66**, 296-302 (1991).
40. H. M. Elsheikha, and L. S. Mansfield, "Assessment of Sarcocystis neurona sporocyst viability and differentiation between viable and nonviable sporocysts using propidium iodide stain," J. Parasitol. **90**, 872-875 (2004).
41. C. Xu, and W. W. Webb, "Measurement of two-photon excitation cross sections of molecular fluorophores with data from 690 to 1050 nm," J. Opt. Soc. Am. B **13**, 481-491 (1996).